



RESEARCH ARTICLE

10.1029/2023JD038570

Chemical Activity of Low Altitude (50 km) Sprite Streamers

Alejandro Malagón-Romero^{1,2} , Francisco J. Pérez-Invernón¹ , and Francisco J. Gordillo-Vázquez¹ 

¹Instituto de Astrofísica de Andalucía (IAA), CSIC, Granada, Spain, ²Centrum Wiskunde & Informatica (CWI), Amsterdam, The Netherlands

Key Points:

- A three-stage approach is proposed to explore the chemical impact of sprite streamers at 50 km
- The main mechanism leading to N₂O is associative detachment during the streamer phase and N + NO₂ → N₂O + O in the long post-streamer phase
- The local increase of NO₂ due to sprite streamers at ~50 km could account for the measurable chemical perturbation of NO₂ over thunderstorms

Supporting Information:

Supporting Information may be found in the online version of this article.

Correspondence to:

A. Malagón-Romero,
malagon@cwi.nl

Citation:

Malagón-Romero, A., Pérez-Invernón, F. J., & Gordillo-Vázquez, F. J. (2023). Chemical activity of low altitude (50 km) sprite streamers. *Journal of Geophysical Research: Atmospheres*, 128, e2023JD038570. <https://doi.org/10.1029/2023JD038570>

Received 26 JAN 2023

Accepted 28 JUN 2023

Abstract A three-stage simulation is used to explore the chemical influence of low altitude (50 km) sprite streamers on the atmosphere, including the chemical trail after the streamer has faded away. In the first stage (streamer phase) a 2D electrodynamic streamer model quantifies the generation of NO_x and N₂O, and the removal of ozone (O₃) by a downward propagating streamer during $\Delta t_{\text{streamer}} = 80 \mu\text{s}$. This streamer propagation leads to a distinctive region in the streamer channel, the glow, where the electric field is enhanced. In the second stage (glow phase), the computed densities of the first stage are used as initial conditions for a 0D model to study the chemical evolution of the streamer channel, where we assume a remanent field of 100 Td for the glow and 0 Td elsewhere. This stage lasts $\Delta t_{\text{glow}} = 85 \mu\text{s}$, the typical glow lifetime at 50 km. Finally, in the third stage (post-streamer phase), we use the same 0D model, switch off the field in the glow region and let the whole streamer wake evolve roughly 100 s ($100 \text{ s} - \Delta t_{\text{glow}}$). Results show a key species such as O₃ is mainly depleted during the streamer phase while NO_x and N₂O are predominantly produced during the same phase. We also compute the local increase of NO₂ by sprite streamers at ~50 km and find out that it could account for the measurable NO₂ anomaly over thunderstorms reported from satellite-based measurements.

Plain Language Summary Sprites are high-altitude electric discharges that occur above thunderstorms and span tens of kilometers vertically and hundreds of meters horizontally. They are made of hundreds of fast-propagating plasma filaments known as streamers. These streamers propagate due to an enhanced electric field at its tip that ionizes the air ahead, leaving behind a chemical trail in the atmosphere. In this work, we focus on the production/removal of prominent greenhouse gases such as N₂O or O₃ as well as nitrogen oxides accounting for the measurable impact of sprites on the low-mesosphere chemistry as reported by satellite-based measurements.

1. Introduction

Sprites are a type of electric discharge known as transient luminous events taking place above thunderstorms (Franz et al., 1990; Gordillo-Vázquez & Pérez-Invernón, 2021; Pasko et al., 1997, 2012; Sentman & Wescott, 1993; Stenbaek-Nielsen et al., 2000; Wilson, 1925). These discharges occur between altitudes of 90 and 40 km in the Earth's mesosphere and are triggered by the quasi-electrostatic field of lightning discharges. A sprite is made of many fast-propagating bright plasma filaments known as streamers. As they travel throughout the atmosphere, streamers branch and interact, and are often followed by long-standing luminous structures, which can persist for 1–100 ms (Stenbaek-Nielsen & McHarg, 2008). These structures are known as beads and glows and are an important part of the sprite phenomenon (Liu, 2010; Luque et al., 2016; Luque & Gordillo-Vázquez, 2010, 2011b; Malagón-Romero et al., 2020). Sprites emit light predominantly in the first and second positive systems of the molecular neutral nitrogen, the first negative system of the molecular nitrogen ion, the Meinel band of the molecular nitrogen ion and the Lyman-Birge-Hopfield (LBH) band of the molecular neutral nitrogen (Armstrong et al., 1998; Chen et al., 2003; Gordillo-Vázquez et al., 2018; Hoder et al., 2016; Ihaddadene & Celestin, 2017; Kanmae et al., 2007; Kuo et al., 2005; Pérez-Invernón, Luque, Gordillo-Vázquez, et al., 2018; Sato et al., 2015; Stenbaek-Nielsen et al., 2007; Šimek, 2014).

Optical diagnostic methods of sprites are used to estimate the plasma characteristics of sprites (Kuo et al., 2019; Malagón-Romero et al., 2019; Pérez-Invernón, Luque, Gordillo-Vázquez, et al., 2018) including the possibility that they could (or not) locally heat up the surrounding atmosphere (Gordillo-Vázquez et al., 2018; Parra-Rojas, Passas, et al., 2013; Pasko et al., 1998). In turn, chemical and electrodynamic models of sprites indicate that they can produce nitrogen oxides (NO_x = NO + NO₂) (Enell et al., 2008; Evtushenko et al., 2013; Gordillo-Vázquez, 2008, 2010; Gordillo-Vázquez et al., 2012; Hiraki et al., 2008; Luque & Gordillo-Vázquez, 2011a; Sentman et al., 2008; Winkler & Nothold, 2014), nitrous oxide (N₂O) (Parra-Rojas et al., 2015; Pérez-Invernón

© 2023. The Authors.

This is an open access article under the terms of the [Creative Commons Attribution-NonCommercial-NoDerivs License](https://creativecommons.org/licenses/by/4.0/), which permits use and distribution in any medium, provided the original work is properly cited, the use is non-commercial and no modifications or adaptations are made.

et al., 2020) and hydrogen oxide radicals ($\text{HO}_x = \text{H} + \text{OH} + \text{HO}_2$) (Winkler et al., 2021; Yamada et al., 2020) in the mesosphere and the lower-ionosphere possibly playing a role in the upper atmospheric budget of ozone. Sentman et al. (2008) estimated a production of 5×10^{19} molecules of NO per sprite-streamer between altitudes 65 and 75 km. Enell et al. (2008) modeled a production of 3×10^{22} – 3×10^{23} molecules of NO per sprite. Pérez-Invernón et al. (2020) estimated an injection of 2×10^{19} molecules of N_2O and 10^{21} molecules of NO per sprite between 68 and 75 km altitude.

The possibility of sprites producing a measurable amount of NO_x at lower sprite altitudes (~ 50 km) motivated Arnone et al. (2008) to search for increases in the concentration of NO_2 above thunderstorms by combining NO_2 measurements from the Michelson Interferometer for Passive Atmospheric Sounding (MIPAS) with lightning measurements from the World Wide Lightning Location Network/Whole Wide Lightning Location Network (WWLLN) between August - December 2003. They reported a statistically significant anomaly in the NO_2 mixing ratio of +1 ppbV at 52 km altitude above thunderstorms over the tropical region. In 2016, Arnone and Dinelli (2016) confirmed the positive anomaly in the mixing ratio of NO_2 above thunderstorms by extending the observing period until April 2004. However, extension of the analysis by Arnone and Dinelli (2016) to the complete data set of MIPAS2D (Dinelli et al., 2010) did not show any significant enhancement in the mixing ratio of NO_2 at 52 km altitude above thunderstorms. These results suggest that the chemical perturbation produced by sprites in the lower mesosphere is at the edge of current detectability.

The inconclusive observations of the increase of NO_2 in the lower mesosphere reported by Arnone et al. (2008) and Arnone and Dinelli (2016) show the need of performing self-consistent chemical and electrodynamical simulations of sprites at about 50 km altitude. In the present work we have followed a three-stage simulation scheme in order to explore the potential of low altitude (~ 50 km) sprite streamer in producing chemical species of atmospheric interest. First, we conducted a 2D electrodynamical simulation (Pérez-Invernón et al., 2020) of a single positive sprite streamer moving downward 250 m, starting at 50 km altitude. The streamer reached the lower boundary at around $\Delta t_{\text{streamer}} = 80 \mu\text{s}$. This simulation served us to quantify the generation of NO_x and N_2O , and the removal of ozone (O_3) by a single streamer. The streamer propagation leaves behind a chemical imprint, the streamer channel, and embedded in it, a glow where the electric field is enhanced. Second, we took the chemical configuration of the streamer channel at the end of the first stage, and used it as initial conditions for a 0D model. We then applied an electric field of 100 Td to the glow region and of 0 Td elsewhere and simulated the chemical activity during $\Delta t_{\text{glow}} = 85 \mu\text{s}$, which is the typical sprite glow lifetime at 50 km. Finally, we switched off the electric field in the glow region and ran a long simulation with the 0D model for roughly 100 s (actually $100 \text{ s} - \Delta t_{\text{glow}}$) to explore the chemical activity of the streamer trail. This three-stage simulation procedure served us to estimate the complete chemical influence of sprites at about 50 km altitude.

2. Methods

In this work, we are interested in the chemical impact of sprite streamers in the lower mesosphere (~ 50 km) for a time scale of tens of seconds. However, a fully self-consistent simulation for such a long time scale is yet computationally unfeasible. To address this issue, we opt to simulate a single sprite streamer and use two different numerical models to study consecutive stages of the streamer evolution: (a) a 2D cylindrically symmetric model to simulate the downward propagation of a single positive sprite streamer, and (b) a 0D model to extend the evolution of the different chemical species in the streamer channel beyond typical streamer propagation time scales.

2.1. 2D Streamer Model

Simulating a sprite is out of reach with current microscopical models due to computational limitations. Instead, we focus on a single streamer in the absence of branching. Under these assumptions, we decided to use a 2D cylindrically symmetric model for streamer discharges to study its propagation. The evolution of electrons and ions is given by the drift-diffusion-reaction equations,

$$\frac{\partial n_s}{\partial t} + \nabla \cdot (\pm n_s \mu_s \mathbf{E} - D_s \nabla n_s) = S_{ph} + C_s, \quad (1)$$

so that for each species s , the magnitudes n_s , μ_s , D_s , and C_s are the corresponding density, mobility, diffusion coefficient and net chemical production. \mathbf{E} is the electrostatic field and S_{ph} the photoionization term that has been

derived from Zhelezniak et al. (1982) and was computed using a Helmholtz approach (Luque et al., 2007). Note that the photoionization source term exclusively affects electrons and O_2^+ . In our approach we consider motionless ions over the time scales that we study and therefore we neglect their mobility and diffusion coefficients. We use the local field approximation and, consequently, transport coefficients are derived from the electron energy distribution function that only depends on the local electric field.

The electrostatic field is irrotational and so it is given by the electrostatic potential ϕ , $\mathbf{E} = -\nabla\phi$. On the other hand, the potential is related to the sources (electric charges) according to Poisson's equation:

$$\nabla^2\phi = -\sum_s \frac{q_s}{\epsilon_0}, \quad (2)$$

where ϵ_0 is the vacuum permittivity and q_s is the electric charge of the species s . Note here that in this model, we will consistently solve Poisson's equation to obtain the electric field due to the charge separation in the streamer. This is a remarkable difference with respect to previous works where the electric field associated with the streamer was a tunable input (Enell et al., 2008; Hiraki et al., 2008; Sentman et al., 2008).

The model consists in a set of hyperbolic (Equation 1) and elliptic (Equation 2) equations. To solve the set of hyperbolic Equation 1 we use Finite Volume Methods (FVMs) (LeVeque, 2002). In particular, our code is built on top of CLAWPACK/PETCLAW (Alghamdi et al., 2011; Clawpack Development Team, 2017; LeVeque, 2002), a collection of FVMs. PETCLAW relies on PETSc (Balay et al., 2016a, 2016b) and allows us to split the simulation domain into different subdomains (problems) that can be solved in parallel. Poisson's Equation 2 is solved using the Generalized Minimal Residual method and the geometric algebraic multigrid preconditioner, both from the PETSc numerical library.

2.1.1. Initial and Boundary Conditions

Sprites are high-altitude discharges made of many streamers that propagate through an air mixture of varying density in which each chemical species has its own chemical profile and relative importance. In this work, the initial state of the atmosphere follows the chemical profiles of Figure 1 of Pérez-Invernón, Luque, and Gordillo-Vázquez (2018), that is, we set the air density profile and composition at nighttime conditions in November from the Whole Atmosphere Community Climate Model (Marsh et al., 2013) for a latitude of 38° and a longitude of 0° relaxed for 6.5 s under the presence of cosmic ray ionization (Thomas, 1974). The concentration of nitrogen atoms (N) is negligible and the humidity is set to zero (dry air conditions). We also set a constant background electron density of $6 \times 10^7 \text{ m}^{-3}$. This value comes from applying scaling laws to typical background electron densities in streamer simulations that range from 10^9 to 10^{15} m^{-3} (Malagón-Romero & Luque, 2018, 2019). On top of that, we add a spherical Gaussian seed (Raizer, 1991) in the uppermost boundary located at 50 km to help triggering the streamer propagation. The seed has an e-folding radius of 5 m which is on the order of the maximum size of the electron avalanche (right before charge effects become important) at 50 km (Köhn et al., 2019). A peak density of $6 \times 10^{12} \text{ m}^{-3}$ sufficed to start the streamer propagation and agrees with typical values for streamer simulations at ground pressure after applying scaling laws (Malagón-Romero & Luque, 2019). This initial electron density is neutralized by an identical density of positive ions, specifically N_2^+ (79%) and O_2^+ (21%).

The unequivocal solution of the equations in our model is subjected to a set of boundary conditions. To solve Poisson's equation we impose zero Dirichlet boundary conditions at $z = z_{\min}$ and $z = z_{\max}$, zero Neumann boundary conditions at the inner radial boundary and free boundary conditions at $r = r_{\max}$ according to the method described by Malagón-Romero and Luque (2018). These free boundary conditions are consistent with the density charge inside the domain and with a potential decaying far away from the source. Likewise, we impose zero Neumann boundary conditions to solve Equation 1.

With the model described in this section, we have simulated the downward propagation of a single positive sprite streamer in a computational domain that starts at $z_{\max} = 50 \text{ km}$ and extends 300 m ($z_{\min} = 49.7 \text{ km}$) vertically and 30 m radially. Note that these dimensions are consistent (Ebert et al., 2010) with maximum single streamer propagation lengths (up to tens of centimeters) at ground pressure (Kochkin et al., 2016). Thus, it is not physically reasonable to follow the propagation of a single streamer for longer distances. The streamer propagates a total of 250 m after $\Delta t_{\text{streamer}} = 80 \mu\text{s}$, moment where we stopped the simulation to avoid any artifacts derived from the interaction between streamer and lower boundary. The background electric field in a sprite is generated by

the charges in the thundercloud below the sprite and the charge transported by interacting streamers. Our model does not account for these details and instead we used a constant and homogeneous background electric field of 0.016 kV/cm. This field corresponds to a reduced field of approximately 80 Td, which is roughly a 33% below the breakdown field, and sufficed to start the streamer propagation.

2.2. 0D Model

The streamer head propagation leaves behind an ionized channel and a chemical imprint in the air admixture. As we argued before, following the propagation of a single streamer beyond 300 m at 50 km altitude is not realistic in the absence of branching. We therefore focus on following just the chemistry in the streamer channel left behind the streamer head. The 0D model is meant to study the activation and chemical evolution of different chemical species at a set of grid-points in the computational domain described in the previous section, where every point is treated independently. In this model we do not consider any charge effects, photoionization or any sort of transport of charged and neutral species. Hence, we set to zero the drift and diffusion terms in Equation 1. The resulting set of equations is of the kind:

$$\frac{\partial n_s}{\partial t} = C_s, \quad (3)$$

following the same notation of Equation 1. This initial value problem for a system of ordinary differential equations can be numerically integrated using, for example, the function `scipy.integrate.solve_ivp` of the python library *SciPy* (<https://scipy.org/about/>). For our calculations we use the implicit Runge-Kutta method of order 5 of the Radau IIA family (Wanner & Hairer, 1996).

2.2.1. Initial Conditions

The streamer wake is a cold plasma channel. The charge distribution left behind by the streamer head can lead to sharply defined, luminous and long lasting columns in the streamer channel known as sprite glows, where the local electric field as well as the chemical activity are enhanced (Luque et al., 2016; Malagón-Romero et al., 2020). It is then, natural, to at least distinguish two well-separated regions in the streamer channel regarding the conditions they are subjected to. The electric field in the streamer glow turns out to be higher than in the rest of the channel. Numerical simulations in the literature as well as the results that will be presented in next sections, agree with observations to a great extent and set a reduced electric field of 100Td in the glow (Luque et al., 2016; Malagón-Romero et al., 2020). During the streamer simulation, the sprite glow appears in the upper part of the streamer channel, specifically in the range (50 km, 49.95 km). For the 0D simulation we take a set of evenly separated points both in the vertical and radial direction of our computational domain. The densities of each species are initiated with the corresponding values resulting from the simulated streamer propagation described in 2.1.1. The simulation extends for a total of 100 s with a time step of 5 ms. As we argued, we assumed a persistent electric field of 100 Td in the glow and for simplicity, zero elsewhere. This persistent electric field lasts $\Delta t_{glow} = 85 \mu s$ and is as follows

$$E/N_{air}(t) = \begin{cases} 100 Td, & \Delta t_{streamer} < t < \Delta t_{streamer} + \Delta t_{glow} \\ 0 Td, & \Delta t_{streamer} + \Delta t_{glow} < t < 100 s \end{cases} \quad (4)$$

where $\Delta t_{streamer} = 80 \mu s$ and $t = \Delta t_{streamer}$ marks the end of the simulation of the streamer propagation (streamer phase). The rest of the points, that is, those that are not contained in the glow, are subjected to a zero background electric field for 100 s starting at $t = \Delta t_{streamer}$. Please note that the $\Delta t_{glow} = 85 \mu s$ duration considered for the sprite streamer wake at about 50 km altitude is consistent with the duration on the order of the millisecond of the electric field in the sprite streamer glow at 70 km (Gordillo-Vázquez & Luque, 2010; Sentman & Stenbaek-Nielsen, 2009) based on observations (Stenbaek-Nielsen & McHarg, 2008). The observations by Stenbaek-Nielsen and McHarg (2008), showed sprite streamer glows with durations up to tens of milliseconds at 83 km. Therefore, applying the scale law $p_{50km} t_{50km}^{glow} = p_{83km} t_{83km}^{glow}$, we obtain that $t_{50km}^{glow} = 85 \mu s$ (assuming $t_{83km}^{glow} = 10 ms$, $p_{50km} = 6.79 \times 10^{-6} atm$, $p_{83km} = 5.18 \times 10^{-6} atm$).

2.3. Chemical Model

We use a modified version of the set of chemical reactions for halos and elves collected in the Appendix of Pérez-Invernón, Luque, and Gordillo-Vázquez (2018), based on sprite and halo models developed in previous

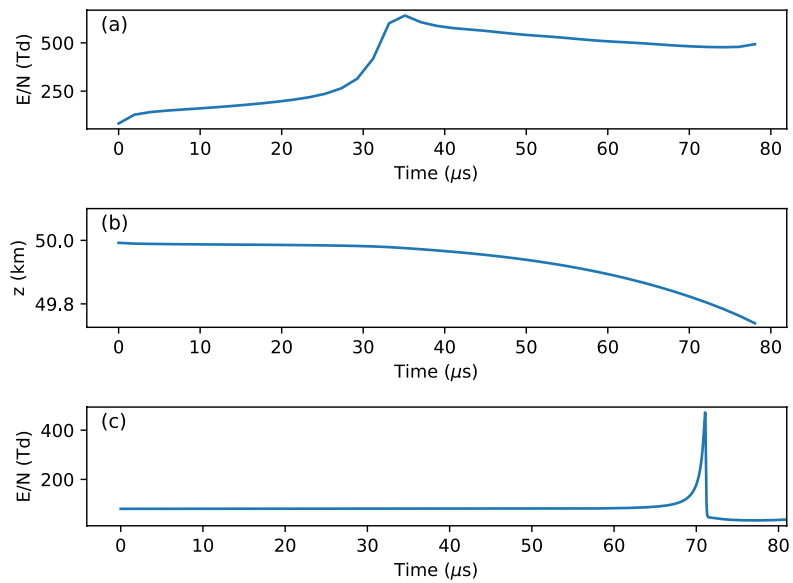


Figure 1. (a) Evolution of the maximum reduced electric field, that is, the electric field at the tip, (b) position of the streamer tip and (c) evolution of the reduced electric field at $r = 0$, $z = 49.82$ km. The “width” of the impulsive streamer shape can be somehow estimated and yields a value of $0.3 \mu\text{s}$.

studies (Gordillo-Vázquez, 2008; Gordillo-Vázquez, 2010; Parra-Rojas et al., 2015; Parra-Rojas, Luque, & Gordillo-Vázquez, 2013; Pérez-Invernón et al., 2020). In addition, the chemical reactions of the 2D model of streamers developed by Malagón-Romero and Luque (2018) are added to the model. As sprite streamers take place in the mesosphere where the concentration of water is negligible, we do not include chemical reactions involving water in our simulation. Vibrational chemistry of CO_2 is not considered in this study.

This vibrational and electronical chemical model allows us to calculate the temporal evolution of the density of $\text{N}_2(B^3\Pi_g, v = 0, \dots, 6)$, $\text{N}_2(C^3\Pi_u, v = 0, \dots, 4)$ and $\text{N}_2(a^1\Pi_g, v = 0, \dots, 15)$.

We have used the software QtPlaskin (Luque, 2011) to analyze the most prominent chemical processes for each of the species of interest.

3. Results and Discussion

3.1. Streamer Propagation Phase

Figure 1 shows the evolution of the maximum reduced electric field (a), which corresponds to the field at the tip of the streamer, the position of the streamer head (b) and finally, the profile of the electric field pulse (c) due to the streamer head passage at $z = 49.82$ km.

Note that the maximum electric field reaches a peak at around $35 \mu\text{s}$ and starts to decrease afterward. There is though a change in this decreasing trend by the end of the simulation (around $80 \mu\text{s}$) and it is not physical. As the streamer head gets closer to the lower boundary of the computational domain, this starts to artificially perturb the streamer propagation. Therefore at $t = 80 \mu\text{s}$ we stop the simulation and this time marks the duration of the streamer phase (first stage). Note that the computational domain size is not casually chosen but consistent (from the point of view of the scaling laws (Ebert et al., 2010)) with the length of long streamers at ground pressure where branching is absent (Kochkin et al., 2016).

As panel (c) of Figure 1 shows, the sprite streamer pulse width at a fixed altitude (49.82 km) resulting from our self-consistent 2D streamer model is of about 0.3 microseconds, which is consistent with previous values assumed at 70 km after applying scaling laws, and those used by Parra-Rojas et al. (2015) (see Figure 3) at 50 km.

Figure 2 shows snapshots of the reduced electric field (a) and the most significant density enhancements (b-h) for a subset of the chemical scheme described in Section 2.3. After $80 \mu\text{s}$, the streamer tip has propagated downwards nearly 250 m, starting at the top of the computational domain located at 50 km.

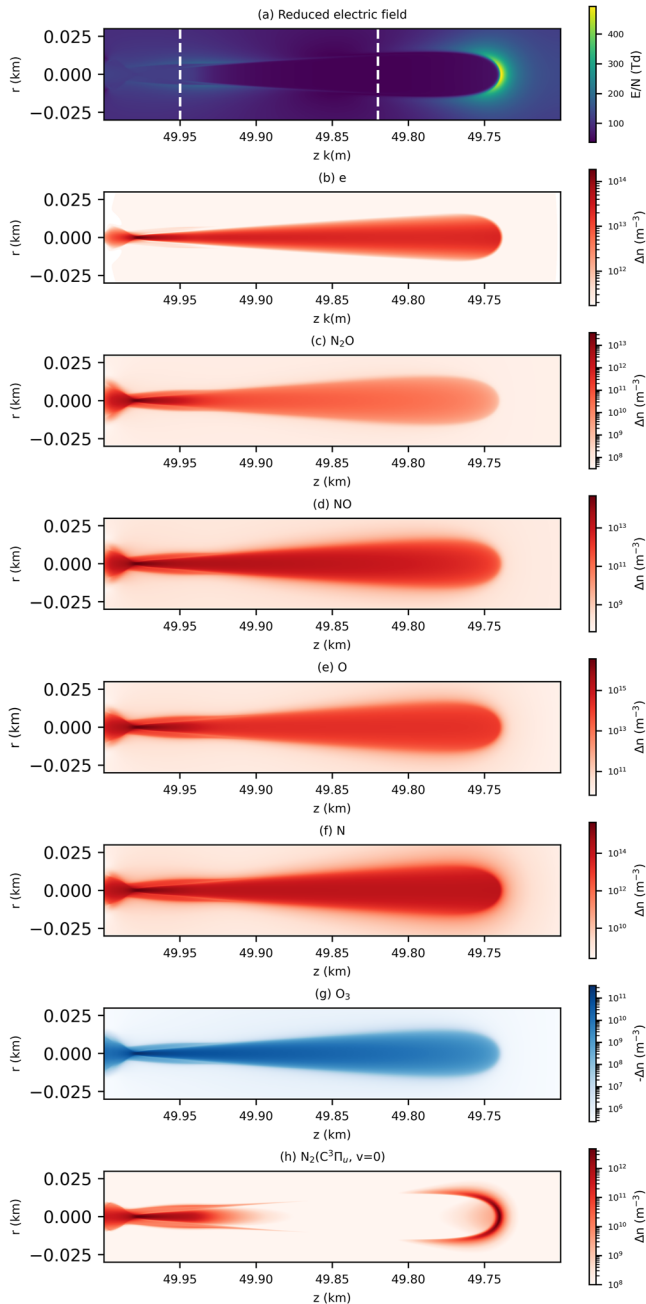


Figure 2. (a) Reduced electric field and (b–h) density enhancement with respect to the background of different chemical species produced by a simulated positive sprite streamer 80 μ s after the onset of the simulation between altitudes 50 and 49.7 km. The white dashed lines in (a) mark the altitudes analyzed in Figure 3.

electron-impact dissociation of N_2 , whose reaction rate is driven by the electric field. This kind of reactions readily produce electronically excited nitrogen states which in turn, contribute to the evolution of NO. It is worth mentioning that, out of all the species shown in Figure 2, the loss mechanisms dominate over the production mechanisms only for O_3 . The effective loss of O_3 is mainly due to dissociative attachment ($e + O_3 \rightarrow O_2 + O^-$) and, in second place, O_3 can also be significantly removed by electronically excited atomic oxygen in quenching reactions.

An inspection of the reduced electric field (Figure 2a) and the density of the emitting species $N_2(C^3\Pi_u, v=0)$ (Figure 2h) reveals the emergence of a glow at around 49.95 km, where the charge separation leads to a locally higher and persistent electric field of nearly 100 Td (see Figure 2a). As a result, the chemical activity in the streamer glow is also enhanced (see Figures 2b–2h) and can have a greater impact in the long term when compared to other regions of the streamer channel. This effect is particularly noticeable for the greenhouse gas N_2O . Figures 3a and 3b show the evolution of the most relevant chemical species in a point inside the glow ($r = 0$, $z = 49.95$ km) and outside of it ($r = 0$, $z = 49.82$ km). These points are highlighted in Figure 2 with white dashed lines. The streamer head reaches the point $z = 49.95$ km ($r = 0$ km) at nearly 40 μ s, as it can be seen in the sudden increase of the species concentrations in Figure 3a. The concentrations of the chemical species increase again after ~ 70 μ s (see Figure 3a), which is consistent with the inception of a glow. The effect of the streamer in the point $z = 49.82$ km ($r = 0$ km) is different. The streamer head reaches this point at about 75 μ s (see Figure 3b).

The main production mechanism of N_2O is the electron associative detachment process $N_2 + O^- \rightarrow e + N_2O$. The production rate is around two orders of magnitude greater in the glow than in the rest of the channel and the streamer head, which explains the enhancement observed in Figure 2c. The second most relevant production mechanism of N_2O is the quenching process $N_2(A^3\Sigma_u^+, v=0) + O_2 \rightarrow O + N_2O$ whose production rate is nevertheless nearly one order of magnitude smaller than the one of electron associative detachment. N_2O removal is enhanced at the streamer head due to the electron ionization of N_2O and in the streamer glow (see Figure 3a) due to reactions involving electronically excited states such as $O(^1D) + N_2O \rightarrow NO + NO$, the conversion of negative and positive ions, for instance, $O^- + N_2O \rightarrow NO^- + NO$ and $N_2^+ + N_2O \rightarrow N_2O + N_2$, among others.

The most relevant chemical paths leading the production of NO are $N(^2D) + O_2 \rightarrow NO + O$, $N(^2D) + O_2 \rightarrow NO + O(^1D)$ and $N(^2P) + O_2 \rightarrow NO + O$. All of them involve electronically excited states that are readily produced under high electric fields. Hence, their most significant production occurs in the glow and the streamer head. The production of NO exceeds the losses by more than 5 orders of magnitude. NO is primarily removed through reactions with electronically excited states, such as $O(^1D) + NO \rightarrow N + O_2$, $N(^2D) + NO \rightarrow N_2 + O$ and $N_2(A^3\Sigma_u^+, v=0) + NO \rightarrow N_2 + NO(A^2\Sigma^+)$, among others (see supplementary material). Note also that electron ionization of NO becomes increasingly important as the electric field in the glow stabilizes its value (see Supporting Information S1).

Atomic oxygen is profusely produced during the streamer propagation either in the streamer head or later in the streamer channel and more abundantly in the glow as Figure 2 shows. The mechanisms accounting for the production of atomic oxygen are electron-impact dissociation reactions, namely, $e + O_2 \rightarrow e + O + O$ and $e + O_2 \rightarrow e + O + O(^1D)$. As we have seen, NO is subsequently produced through reactions involving nitrogen excited states and molecular oxygen. On the other hand, nitrogen atoms result from

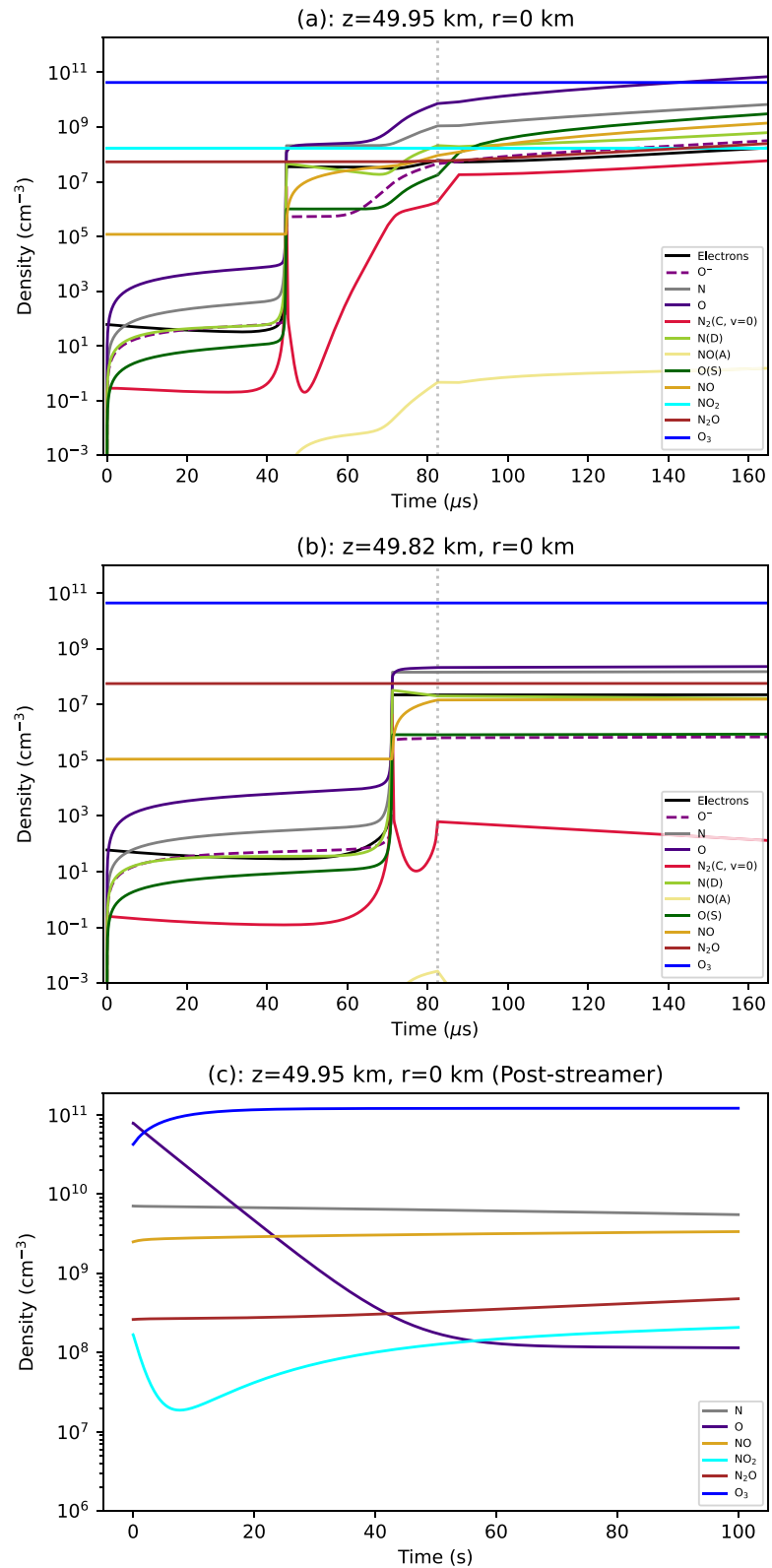


Figure 3. Temporal evolution of the densities of the most important species at different points during the streamer propagation and glow phases (a and b) and the post-streamer phase (c). The vertical dashed line of panels (a and b) indicates the transition from the first stage (streamer phase) to the second stage (glow phase) of the simulation.

Table 1
Chemical Influence of the Different Phases of a Simulated Sprite Streamer on the Concentration of Different Chemical Species Between 50 and 49.7 km

Species	Total number of produced atoms/molecules		
	Streamer phase	Streamer phase + glow phase + post-streamer phase	Streamer phase + post-streamer phase
NO	6.7×10^{17}	7.5×10^{18}	3.1×10^{18}
NO ₂	0.0	2.6×10^{18}	2.9×10^{18}
N ₂ O	6.3×10^{15}	2.6×10^{18}	2.0×10^{18}
O ₃	-4.3×10^{14}	-3.1×10^{22}	-2.0×10^{22} ^a

3.2. Glow Phase

As we explained in Section 2.2.1, the streamer glow phase corresponds to the 85 μs right after the streamer phase where we apply a reduced electric field of 100 Td (Luque & Ebert, 2010; Luque et al., 2016; Malagón-Romero et al., 2020) in the points inside the emerged glow (from 50 to 49.9 km) and 0 Td elsewhere. The obtained temporal evolution of the most important chemical species is shown in Figure 3 for a point inside the glow (a) and another point in the streamer channel but outside the glow (b). The production and loss mechanisms are the same as those observed during the streamer propagation phase, since they are driven by an applied reduced electric field of 100 Td. The most relevant effect of the glow phase in the production of chemical species is the contribution to a second increase in the concentrations of the species under consideration in this work.

3.3. Post-Streamer Phase

The simulation of the post-streamer phase is a continuation of the previous phases and extends 100 s–85 μs immediately after the glow phase with a deactivated background electric field. This simulation serves us to quantify the total chemical influence of the streamer, as it accounts for the evolution of the concentration of chemical species until equilibrium with ambient species is reached. The temporal evolution of the chemical species is shown in Figure 3c. In addition, Table 1 shows the total injection of key chemical species during the streamer propagation phase (second column) and the total simulation time (third column). Alternatively, we show in the fourth column the total injection of chemical species by removing the glow phase (85 μs) in order to estimate the uncertainty introduced by the simulation of the glow.

The atomic nitrogen N produced during the streamer and the glow phase by electron impact dissociation contributes to the increase in the concentration of NO during the post-streamer phase through the chemical reaction $N + O_2 \rightarrow NO + O_2$. In turn, the increase in the concentration of NO produces an enhancement in the concentration of NO₂ (see Table 1) and a subsequent decrease in the concentration of O₃ (see Table 1) driven by the chemical reaction $NO + O_3 \rightarrow NO_2 + O_2$. Despite the total increase in the concentration of NO₂, it is important to note that the concentration of NO₂ decreases during the first 5 s of simulation (see Figure 3c) because the atomic oxygen O produced during the streamer and the glow propagation contributes to a significant removal of NO₂ through the reaction $O + NO_2 \rightarrow O_2 + NO$. However, the high rate of oxygen atom (O) removal deactivates this process after ~5 s. Finally, during the roughly 100 s of the equilibrium phase, the production of NO₂ promotes a slow but continuous increase in the concentration of N₂O led by the process $N + NO_2 \rightarrow O + N_2O$.

The total injection of NO_x per sprite can be estimated from the results presented in this work in the lower mesosphere (50 km) and from Pérez-Invernón et al. (2020) in the mid mesosphere (67–75 km). The chemical influence of sprites in the range of altitude between 50 and 67 km is estimated by interpolating the production and depletion of molecules per meter obtained in the lower mesosphere and in the mid mesosphere, respectively. The chemical influence in the range of altitudes between 45 and 49.75 km is extrapolated from the same values. In particular, one single sprite streamer is predicted to produce 7.5×10^{18} NO molecules per kilometer altitude between 67 and 75 km (Pérez-Invernón et al., 2020), while the production of NO₂ at this range of altitudes is negligible. In turn, one single sprite streamer is predicted to produce 3.0×10^{16} NO molecules and 1.0×10^{16} NO₂ molecules per kilometer altitude between 49.75 and 50 km (Table 1). According to these modeling results, a single sprite streamer would inject about 6.2×10^{20} NO molecules and 2.6×10^{19} NO₂ molecules in the range of altitude between 45 and 75 km. Finally, a conversion factor between the injection of molecules by one single sprite streamer and the total injection of molecules by a complete sprite is needed to parameterize the injection of NO_x. Pérez-Invernón et al. (2020) compared the simulated optical emissions of one single sprite streamer with measurements from space and concluded that a complete sprite emits between 18 and 50 times more photons than the simulated for one single streamer. This leads to a complete production of 1.2×10^{22} – 3.2×10^{22} NO_x molecules, falling at the lower end of the range of estimations by Enell et al. (2008) (Table 1).

We can now approximately estimate the number of sprites needed to reproduce the ~1 ppbv increase in the NO₂ mixing ratio at ~50 km altitude reported by Arnone et al. (2008) within a tropical region volume of 400 ×

30 × 3 km over thunderstorms observed by MIPAS during 20 min before 22 hr local time. Considering that asprite streamers starting at 50 km could move downwards up to ~3 km long reaching a mean radius of up to ~0.045 km or more (Gerken et al., 2000; Stenbaek-Nielsen & McHarg, 2008), the local NO₂ impact of low altitude sprite streamers can be estimated if we consider that: (a) the peak density enhancement of 4 × 10⁸ cm⁻³ for NO due to the streamer head passage is further increased up to 4 × 10⁹ cm⁻³ (see Figures 3b and 3c) during the sprite glow and the sprite equilibrium phase (of 100 s), (b) the volume occupied by 1 streamer ($R = 0.045$ km, $H = 3$ km) is $V_{streamer} = 0.019$ km³, (c) the volume occupied by 1 sprite (with some hundreds of streamers, say ~200 streamers) is $200 \times V_{streamer} = 3.82$ km³, (d) the ratio r between the volume occupied by 1 sprite and the volume of the region sounded by MIPAS in Arnone et al. (2008) is $r = 8.4 \times 10^{-5}$, (e) the density of the air at 50 km altitude is 1.94×10^{16} cm⁻³. Therefore, the increase of the density of NO₂ diluted over the entire MIPAS volume due to sprite activity is 4×10^9 cm⁻³ × 8.4×10^{-5} = 3.36×10^5 cm⁻³, and the total number of sprites needed to produce the observed ~1 ppbv increase of NO₂ at 50 km altitude is $\sim 1.94 \times 10^{16}$ cm⁻³ × $1.0 \times 10^{-9}/3.36 \times 10^5$ cm⁻³ = 58 sprites.

Considering that the estimates of the global rate of sprite occurrence range between 0.5/min (Sato & Fukunishi, 2003), 1/min (Chen et al., 2008), 3/min Ignaccolo et al. (2006), and 33/min (Blanc et al., 2004; Yair et al., 2004). We assume, following Ignaccolo et al. (2006) and Arnone et al. (2014), 3 sprites/min (about 1 sprite every approximately 1,000 lightning flashes, which rates at about 45/s in Christian et al. (2003)), which gives about 60 sprites occurring worldwide during 20 min. However, sprites only occur over some storms out of the total number of active storms at a given time and, most probably, there will be one or two of those sprite producing storms in the MIPAS sounded volume reported in Arnone et al. (2008), which also reported that their NO₂ observations (above thunderstorms) was consistent with only 10% of the lightning flashes observed by the WWLLN. Therefore, at the level of order of magnitude, we can reasonably consider that the NO₂ computed in this work produced by low altitude (50 km) sprite streamers, their glows and equilibrium phases could well explain the observed ~1 ppbv NO₂ enhancement at ~50 km reported by Arnone et al. (2008).

We consider that microscopic sprite streamer simulations at different altitudes are a needed step to build accurate sprite parameterizations that, appropriately coupled into chemistry-climate models, could provide a new approach to understand and quantify the sprite chemical influence in the atmosphere. Comparison of chemistry-climate models including sprites with global and/or regional observations of chemical enhancements over stormy weather regions is therefore the next important step.

4. Summary and Conclusions

We have followed a three-stage simulation approach to explore the local chemical influence of low altitude (50 km) sprite streamers including the chemical wake after streamers have faded away. First, a 2D electrodynamic simulation was performed to quantify the generation of NO_x and N₂O, and the removal of ozone (O₃) by a downward (50–49.75 km) moving streamer during $\Delta t_{streamer} = 80$ μs. Second, the chemical activity of the streamer channel was simulated during $\Delta t_{glow} = 85$ μs, following the previous streamer phase (80 μs) and using a 0D model with a constant (undervoltage) electric field of 100 Td applied to the glow and of 0Td elsewhere. Finally, a long run (100 s– Δt_{glow}) 0D simulation was carried out to explore the chemical activity of the streamer trail. The main findings of this work are.

1. The injection of nitrogen oxides (NO_x) and nitrous oxide (N₂O) molecules per streamer (NO: 6.7×10^{17} , NO₂: 0 and N₂O: 6.3×10^{15}) are considerable smaller than those resulting from three-stage simulations (NO: 7.5×10^{18} , NO₂: 2.6×10^{18} and N₂O: 2.6×10^{18}).
2. The three-stage simulation scheme yields a local removal of -3.1×10^{22} molecules of O₃.
3. The local increase of NO₂ due to sprite streamers at ~50 km could account for the measurable chemical perturbation of NO₂ over thunderstorms previously reported by Arnone et al. (2008) at the edge of current detectability.
4. The comparison of observations of chemical anomalies over stormy weather regions with global and/or regional chemistry-climate models (that incorporate accurate sprite parameterizations) can contribute to definitively clarify the chemical impact of the sprite activity in the atmosphere.
5. The main mechanism leading to N₂O is associative detachment during the streamer phase and $N + NO_2 \rightarrow N_2O + O$ in the long post-streamer phase.

Data Availability Statement

The data set for this research is available in this in-text data citation reference (Malagón-Romero et al., 2022), under a Creative Commons Attribution 4.0 International license and available at the time of submission. Such data set is findable and accessible at <https://zenodo.org/record/7049908>. The code developed for the simulation of sprite streamers is available at <https://gitlab.com/amaro/streamer2d>.

Acknowledgments

This work was supported by the Spanish Ministry of Science and Innovation under project PID2019-109269RB-C43 and the FEDER program, and by Junta de Andalucía under project PY20-00831. AM acknowledges a postdoctoral contract under project PY20-00831 and the financial support of Ramón Areces Foundation. FJPI acknowledges the sponsorship provided by Junta de Andalucía under Grant POSTDOC-21-00052 and “la Caixa” Foundation (ID 10001043) with fellowship code LCF/BQ/PI22/11910026. FJPI and FJGV acknowledge financial support from the grant CEX2021-001131-S funded by MCIN/AEI/10.13039/501100011033. The high performance computer simulations of this work were carried in the MareNostrum Supercomputer under project number FI-2021-1-0040 granted by the Barcelona Supercomputing Center.

References

- Alghamdi, A., Ahmadi, A., Ketcheson, D. I., Knepley, M. G., Mandli, K. T., & Dalcin, L. (2011). PetClaw: A scalable parallel nonlinear wave propagation solver for Python. In *Proceedings of the 19th High Performance Computing Symposia* (pp. 96–103). Society for Computer Simulation International. Retrieved from <http://dl.acm.org/citation.cfm?id=2048577.2048590>
- Armstrong, R. A., Shorter, J. A., Taylor, M. J., Suszcynsky, D. M., Lyons, W. A., & Jeong, L. S. (1998). Photometric measurements in the SPRITES 1995 and 1996 campaigns of nitrogen second positive (399.8 nm) and first negative (427.8 nm) emissions. *Journal of Atmospheric and Solar-Terrestrial Physics*, *60*(7–9), 787–799. [https://doi.org/10.1016/S1364-6826\(98\)00026-1](https://doi.org/10.1016/S1364-6826(98)00026-1)
- Arnone, E., & Dinelli, B. M. (2016). CHIMTEA—Chemical impact of thunderstorms on Earth’s atmosphere. In *Remote Sensing Advances for Earth System Science* (pp. 1–14). Springer.
- Arnone, E., Kero, A., Dinelli, B. M., Enell, C.-F., Arnold, N. F., Papandrea, E., et al. (2008). Seeking sprite-induced signatures in remotely sensed middle atmosphere NO₂. *Geophysical Research Letters*, *35*(5), L05807. <https://doi.org/10.1029/2007GL031791>
- Arnone, E., Smith, A. K., Enell, C.-F., Kero, A., & Dinelli, B. M. (2014). WACCM climate chemistry sensitivity to sprite perturbations. *Journal of Geophysical Research: Atmospheres*, *119*(11), 6958–6970. <https://doi.org/10.1002/2013JD020825>
- Balay, S., Abhyankar, S., Adams, M. F., Brown, J., Brune, P., Buschelman, K., et al. (2016a). *PETSc users manual (Tech. Rep. No. ANL-95/11 - Revision 3.7)*. Argonne National Laboratory. Retrieved from <http://www.mcs.anl.gov/petsc>
- Balay, S., Abhyankar, S., Adams, M. F., Brown, J., Brune, P., Buschelman, K., et al. (2016b). PETSc Web page. Retrieved from <http://www.mcs.anl.gov/petsc>
- Blanc, E., Farges, T., Roche, R., Brebion, D., Hua, T., Labarthe, A., & Melnikov, V. (2004). Nadir observations of sprites from the international space station. *Journal of Geophysical Research*, *109*(A2). <https://doi.org/10.1029/2003ja009972>
- Chen, A. B., Kuo, C.-L., Lee, Y.-J., Su, H.-T., Hsu, R.-R., Chern, J.-L., et al. (2008). Global distributions and occurrence rates of transient luminous events. *Journal of Geophysical Research*, *113*(A8), A08306. <https://doi.org/10.1029/2008JA013101>
- Chen, A. B., Wang, T., Huang, T., Kuo, C., Hsu, R., Su, H., et al. (2003). *Observations of transient luminous events on the ROCSAT-2 satellite using ISUAL instruments* (p. A792). AGU Fall Meeting Abstracts.
- Christian, H. J., Blakeslee, R. J., Boccippio, D. J., Boeck, W. L., Buechler, D. E., Driscoll, K. T., & Stewart, M. F. (2003). Global frequency and distribution of lightning as observed from space by the Optical Transient Detector. *Journal of Geophysical Research*, *108*(D10), 4005. <https://doi.org/10.1029/2002JD002347>
- Clawpack Development Team. (2017). Clawpack software (version 5.4.1). <https://doi.org/10.5281/zenodo.820730>
- Dinelli, B. M., Arnone, E., Brizzi, G., Carlotti, M., Castelli, E., Magnani, L., et al. (2010). The MIPAS2D database of MIPAS/ENVISAT measurements retrieved with a multi-target 2-dimensional tomographic approach. *Atmospheric Measurement Techniques*, *3*(2), 355–374. <https://doi.org/10.5194/amt-3-355-2010>
- Ebert, U., Nijdam, S., Li, C., Luque, A., Briels, T., & van Veldhuizen, E. (2010). Review of recent results on streamer discharges and discussion of their relevance for sprites and lightning. *Journal of Geophysical Research (Space Physics)*, *115*(A2), A00E43. <https://doi.org/10.1029/2009JA014867>
- Enell, C.-F., Arnone, E., Adachi, T., Chanrion, O., Verronen, P. T., Seppälä, A., et al. (2008). Parameterisation of the chemical effect of sprites in the middle atmosphere. *Annales Geophysicae*, *26*(1), 13–27. <https://doi.org/10.5194/angeo-26-13-2008>
- Evtushenko, A. A., Kuterin, F. A., & Mareev, E. A. (2013). A model of sprite influence on the chemical balance of mesosphere. *Journal of Atmospheric and Terrestrial Physics*, *102*, 298–310. <https://doi.org/10.1016/j.jastp.2013.06.005>
- Franz, R. C., Nemzek, R. J., & Winckler, J. R. (1990). Television image of a large upward electrical discharge above a thunderstorm system. *Science*, *249*(4964), 48–51. <https://doi.org/10.1126/science.249.4964.48>
- Gerken, E. A., Inan, U. S., & Barrington-Leigh, C. P. (2000). Telescopic imaging of sprites. *Geophysical Research Letters*, *27*(17), 2637–2640. <https://doi.org/10.1029/2000GL000035>
- Gordillo-Vázquez, F. J. (2008). Air plasma kinetics under the influence of sprites. *Journal of Physics D*, *41*(23), 234016. <https://doi.org/10.1088/0022-3727/41/23/234016>
- Gordillo-Vázquez, F. J. (2010). Vibrational kinetics of air plasmas induced by sprites. *Journal of Geophysical Research*, *115*(A5), A00E25. <https://doi.org/10.1029/2009JA014688>
- Gordillo-Vázquez, F. J., & Luque, A. (2010). Electrical conductivity in sprite streamer channels. *Geophysical Research Letters*, *37*(16), L16809. <https://doi.org/10.1029/2010GL044349>
- Gordillo-Vázquez, F. J., Luque, A., & Simek, M. (2012). Near infrared and ultraviolet spectra of TLEs. *Journal of Geophysical Research*, *117*(A5), A05329. <https://doi.org/10.1029/2012ja017516>
- Gordillo-Vázquez, F. J., Passas, M., Luque, A., Sánchez, J., Velde, O. A., & Montanyá, J. (2018). High spectral resolution spectroscopy of sprites: A natural probe of the mesosphere. *Journal of Geophysical Research: Atmospheres*, *123*(4), 2336–2346. <https://doi.org/10.1002/2017jd028126>
- Gordillo-Vázquez, F. J., & Pérez-Invernón, F. J. (2021). A review of the impact of transient luminous events on the atmospheric chemistry: Past, present, and future. *Atmospheric Research*, *252*, 105432. <https://doi.org/10.1016/j.atmosres.2020.105432>
- Hiraki, Y., Kasai, Y., & Fukunishi, H. (2008). Chemistry of sprite discharges through ion-neutral reactions. *Atmospheric Chemistry and Physics*, *8*(14), 3919–3928. <https://doi.org/10.5194/acp-8-3919-2008>
- Hoder, T., Simek, M., Bonaventura, Z., Prukner, V., & Gordillo-Vázquez, F. J. (2016). Radially and temporally resolved electric field of positive streamers in air and modelling of the induced plasma chemistry. *Plasma Sources Science and Technology*, *25*(4), 045021. <https://doi.org/10.1088/0963-0252/25/4/045021>
- Ignaccolo, M., Farges, T., Mika, A., Allin, T. H., Chanrion, O., Blanc, E., et al. (2006). The Planetary rate of sprite events. *Geophysical Research Letters*, *33*(11), L11808. <https://doi.org/10.1029/2005GL025502>
- lhaddadene, M. A., & Celestin, S. (2017). Determination of sprite streamers altitude based on N₂ spectroscopic analysis. *Journal of Geophysical Research: Space Physics*, *122*(1), 1000–1014. <https://doi.org/10.1002/2016ja023111>

- Kanmae, T., Stenbaek-Nielsen, H. C., & McHarg, M. G. (2007). Altitude resolved sprite spectra with 3 ms temporal resolution. *Geophysical Research Letters*, 34(7), L07810. <https://doi.org/10.1029/2006GL028608>
- Kochkin, P., Lehtinen, N., van Deursen, A. L. P. J., & Østgaard, N. (2016). Pilot system development in metre-scale laboratory discharge. *Journal of Physics D: Applied Physics*, 49(42), 425203. <https://doi.org/10.1088/0022-3727/49/42/425203>
- Köhn, C., Chanrion, O., & Neubert, T. (2019). The sensitivity of sprite streamer inception on the initial electron-ion patch. *Journal of Geophysical Research: Space Physics*, 124(4), 3083–3099. <https://doi.org/10.1029/2018JA025972>
- Kuo, C.-L., Chou, J.-K., Wu, Y.-J., Williams, E., Chen, A. B.-C., Su, H.-T., et al. (2019). The Boltzmann vibrational temperature of $N_2(B^3\Pi_g)$ derived from ISUAL imager multiband measurements of transient luminous events. *Journal of Geophysical Research: Space Physics*, 124(12), 10760–10777. <https://doi.org/10.1029/2019JA027311>
- Kuo, C.-L., Hsu, R. R., Chen, A. B., Su, H. T., Lee, L. C., Mende, S. B., et al. (2005). Electric fields and electron energies inferred from the ISUAL recorded sprites. *Geophysical Research Letters*, 32(19), L19103. <https://doi.org/10.1029/2005GL023389>
- LeVeque, R. (2002). *Finite volume methods for hyperbolic problems*. Cambridge University Press.
- Liu, N. (2010). Model of sprite luminous trail caused by increasing streamer current. *Geophysical Research Letters*, 37(4), L04102. <https://doi.org/10.1029/2009GL042214>
- Luque, A. (2011). Computer code QTPlaskin. Retrieved from <https://github.com/aluque/qtplaskin>
- Luque, A., & Ebert, U. (2010). Sprites in varying air density: Charge conservation, glowing negative trails and changing velocity. *Geophysical Research Letters*, 37(6), L06806. <https://doi.org/10.1029/2009GL041982>
- Luque, A., Ebert, U., Montijn, C., & Hundsdoerfer, W. (2007). Photoionization in negative streamers: Fast computations and two propagation modes. *Applied Physics Letters*, 90(8), 081501. <https://doi.org/10.1063/1.2435934>
- Luque, A., & Gordillo-Vázquez, F. (2010). *Modeling of sprite beads: Using numerical streamer simulations to infer the pre-existing electron density in a sprite discharge*. AGU Fall Meeting Abstracts.
- Luque, A., & Gordillo-Vázquez, F. J. (2011a). Modeling and analysis of $N_2(B^3\Pi_g)$ and $N_2(C^3\Pi_u)$ vibrational distributions in sprites. *Journal of Geophysical Research*, 116(A2), A02306. <https://doi.org/10.1029/2010JA015952>
- Luque, A., & Gordillo-Vázquez, F. J. (2011b). Sprite beads originating from inhomogeneities in the mesospheric electron density. *Geophysical Research Letters*, 38(4), L04808. <https://doi.org/10.1029/2010GL046403>
- Luque, A., Stenbaek-Nielsen, H., McHarg, M., & Haaland, R. (2016). Sprite beads and glows arising from the attachment instability in streamer channels. *Journal of Geophysical Research: Space Physics*, 121(3), 2431–2449. <https://doi.org/10.1002/2015ja022234>
- Malagón-Romero, A., & Luque, A. (2018). A domain-decomposition method to implement electrostatic free boundary conditions in the radial direction for electric discharges. *Computer Physics Communications*, 225, 114–121. <https://doi.org/10.1016/j.cpc.2018.01.003>
- Malagón-Romero, A., & Luque, A. (2019). Spontaneous emergence of space stems ahead of negative leaders in lightning and long sparks. *Geophysical Research Letters*, 46(7), 4029–4038. <https://doi.org/10.1029/2019GL082063>
- Malagón-Romero, A., Pérez-Invernón, F., & Gordillo-Vázquez, F. J. (2022). *Sprite streamer at 50 km altitude*. Zenodo. <https://doi.org/10.5281/zenodo.7049908>
- Malagón-Romero, A., Pérez-Invernón, F. J., Luque, A., & Gordillo-Vázquez, F. J. (2019). Analysis of the spatial nonuniformity of the electric field in spectroscopic diagnostic methods of atmospheric electricity phenomena. *Journal of Geophysical Research: Atmospheres*, 124(22), 12356–12370. <https://doi.org/10.1029/2019JD030945>
- Malagón-Romero, A., Teunissen, J., Stenbaek-Nielsen, H. C., McHarg, M. G., Ebert, U., & Luque, A. (2020). On the emergence mechanism of carrot sprites. *Geophysical Research Letters*, 47(1), e85776. <https://doi.org/10.1029/2019GL085776>
- Marsh, D. R., Mills, M. J., Kinnison, D. E., Lamarque, J. F., Calvo, N., & Polvani, L. M. (2013). Climate change from 1850 to 2005 simulated in CESM1 (WACCM). *Journal of Climate*, 26(19), 7372–7391. <https://doi.org/10.1175/JCLI-D-12-00558.1>
- Parra-Rojas, F. C., Luque, A., & Gordillo-Vázquez, F. J. (2013). Chemical and electrical impact of lightning on the Earth mesosphere: The case of sprite halos. *Journal of Geophysical Research*, 118(8), 1–25. <https://doi.org/10.1002/jgra.50449>
- Parra-Rojas, F. C., Luque, A., & Gordillo-Vázquez, F. J. (2015). Chemical and thermal impact of sprite streamers in the Earth mesosphere. *Journal of Geophysical Research: Space Physics*, 120(10), 8899–8933. <https://doi.org/10.1002/2014JA020933>
- Parra-Rojas, F. C., Passas, M., Carrasco, E., Luque, A., Tanarro, I., Simek, M., & Gordillo-Vázquez, F. J. (2013). Spectroscopic diagnostics of laboratory air plasmas as a benchmark for spectral rotational (gas) temperature determination in TLEs. *Journal of Geophysical Research*, 118(7), 4649–4661. <https://doi.org/10.1002/jgra.50433>
- Pasko, V. P., Inan, U. S., & Bell, T. F. (1998). Spatial structure of sprites. *Geophysical Research Letters*, 25(12), 2123–2126. <https://doi.org/10.1029/98GL01242>
- Pasko, V. P., Inan, U. S., Bell, T. F., & Taranenko, Y. N. (1997). Sprites produced by quasi-electrostatic heating and ionization in the lower ionosphere. *Journal of Geophysical Research*, 102(A3), 4529–4561. <https://doi.org/10.1029/96JA03528>
- Pasko, V. P., Yair, Y., & Kuo, C.-L. (2012). Lightning related transient luminous events at high altitude in the Earth's atmosphere: Phenomenology, mechanisms and effects. *Space Science Reviews*, 168(1–4), 475–516. <https://doi.org/10.1007/s11214-011-9813-9>
- Pérez-Invernón, F. J., Luque, A., & Gordillo-Vázquez, F. J. (2018a). Modeling the chemical impact and the optical emissions produced by lightning-induced electromagnetic fields in the upper atmosphere: The case of Halos and Elves triggered by different lightning discharges. *Journal of Geophysical Research: Atmospheres*, 123(14), 7615–7641. <https://doi.org/10.1029/2017JD028235>
- Pérez-Invernón, F. J., Luque, A., Gordillo-Vázquez, F. J., Sato, M., Ushio, T., Adachi, T., & Chen, A. B. (2018). Spectroscopic diagnostic of halos and elves detected from space-based photometers. *Journal of Geophysical Research: Atmospheres*, 123(22), 12917–12941. <https://doi.org/10.1029/2018JD029053>
- Pérez-Invernón, F. J., Malagón-Romero, A., Gordillo-Vázquez, F. J., & Luque, A. (2020). The contribution of sprite streamers to the chemical composition of the mesosphere-lower thermosphere. *Geophysical Research Letters*, 47(14), e2020GL088578. <https://doi.org/10.1029/2020GL088578>
- Raizer, Y. P. (1991). *Gas discharge physics*. Springer-Verlag.
- Sato, M., & Fukunishi, H. (2003). Global sprite occurrence locations and rates derived from triangulation of transient Schumann resonance events. *Geophysical Research Letters*, 30(16), 1859. <https://doi.org/10.1029/2003gl017291>
- Sato, M., Ushio, T., Morimoto, T., Kikuchi, M., Kikuchi, H., Adachi, T., et al. (2015). Overview and early results of the global lightning and sprite measurements mission. *Journal of Geophysical Research: Atmospheres*, 120(9), 3822–3851. <https://doi.org/10.1002/2014jd022428>
- Sentman, D. D., & Stenbaek-Nielsen, H. C. (2009). Chemical effects of weak electric fields in the trailing columns of sprite streamers. *Plasma Sources Science and Technology*, 18(3), 034012. <https://doi.org/10.1088/0963-0252/18/3/034012>
- Sentman, D. D., Stenbaek-Nielsen, H. C., McHarg, M. G., & Morrill, J. S. (2008). Plasma chemistry of sprite streamers. *Journal of Geophysical Research*, 113(D11), D11112. <https://doi.org/10.1029/2007JD008941>

- Sentman, D. D., & Wescott, E. M. (1993). Observations of upper atmospheric optical flashes recorded from an aircraft. *Geophysical Research Letters*, 20(24), 2857–2860. <https://doi.org/10.1029/93GL02998>
- Šimek, M. (2014). Optical diagnostics of streamer discharges in atmospheric gases. *Journal of Physics D: Applied Physics*, 47(46), 463001. <https://doi.org/10.1088/0022-3727/47/46/463001>
- Stenbaek-Nielsen, H. C., & McHarg, M. G. (2008). High time-resolution sprite imaging: Observations and implications. *Journal of Physics D*, 41(23), 234009. <https://doi.org/10.1088/0022-3727/41/23/234009>
- Stenbaek-Nielsen, H. C., McHarg, M. G., Kanmae, T., & Sentman, D. D. (2007). Observed emission rates in sprite streamer heads. *Geophysical Research Letters*, 34(11), L11105. <https://doi.org/10.1029/2007GL029881>
- Stenbaek-Nielsen, H. C., Moudry, D. R., Wescott, E. M., Sentman, D. D., & Sao Sabbas, F. T. (2000). Sprites and possible mesospheric effects. *Geophysical Research Letters*, 27(23), 3829–3832. <https://doi.org/10.1029/2000GL003827>
- Thomas, L. (1974). Recent developments and outstanding problems in the theory of the D region. *Radio Science*, 9(2), 121–136. <https://doi.org/10.1029/rs009i002p00121>
- Wanner, G., & Hairer, E. (1996). *Solving ordinary differential equations II* (Vol. 375). Springer Berlin Heidelberg.
- Wilson, C. T. R. (1925). The electric field of a thundercloud and some of its effects. *Proceedings of the Physical Society, London*, 37(1), 32D–37D. <https://doi.org/10.1088/1478-7814/37/1/314>
- Winkler, H., & Nothold, J. (2014). The chemistry of daytime sprite streamers - A model study. *Atmospheric Chemistry and Physics*, 14(7), 3545–3556. <https://doi.org/10.5194/acp-14-3545-2014>
- Winkler, H., Yamada, T., Kasai, Y., Berger, U., & Notholt, J. (2021). Model simulations of chemical effects of sprites in relation with observed HO₂ enhancements over sprite-producing thunderstorms. *Atmospheric Chemistry and Physics*, 21(10), 7579–7596. <https://doi.org/10.5194/acp-21-7579-2021>
- Yair, Y., Israelevich, P., Devir, A. D., Moalem, M., Price, C., Joseph, J. H., & Teller, A. (2004). New observations of sprites from the space shuttle. *Journal of Geophysical Research*, 109(D15), D15201. <https://doi.org/10.1029/2003JD004497>
- Yamada, T., Sato, T., Adachi, T., Winkler, H., Kuribayashi, K., Larsson, R., et al. (2020). HO generation above sprite-producing thunderstorms derived from low-noise smiles observation spectra. *Geophysical Research Letters*, 47(3), e60090. <https://doi.org/10.1029/2019gl085529>
- Zhelezniak, M. B., Mnatsakanian, A. K., & Sizykh, S. V. (1982). Photoionization of nitrogen and oxygen mixtures by radiation from a gas discharge. *Teplotfizika Vysokikh Temperatur*, 20, 423.